Research Paper

Mapping the Flood Inundation Area for Climate Adaptation Planning:

A Chinese Case in Xinxiang City, Henan Province China

Xiaoling Qin, South China University of Technology, China
Meng Meng, South China University of Technology, China
Shifu Wang, South China University of Technology, China

Abstract

With global warming, rising sea levels, and more frequent extreme rainfall events, the need for flood climate adaptation planning has become more urgent. At present, there are relatively few planning studies from the perspective of rainstorm climate adaptation in China. In this study, the Sentinel-1 Multi-Temporal Synthetic Aperture Radar (SAR) was used to monitor the urban flood area from the extreme rainfall weather caused by storm surges. Optical remote sensing is not effective on rainy days. However, Synthetic Aperture Radar (SAR) can penetrate the clouds and obtain optical high-resolution radar images, which can be observed all day long. This method is used to identify the spatial distribution of the flood inundation area of extreme rainfall caused by rainstorm in Xinxiang City, Henan Province. The significance of this study is as follows: (1) Based on data-driven, it provides an operable technical process and method for rainstorm hazard mapping for non-flood plains in China, which can be applied to rainwater hazard mapping of other areas and enhance the science of decision-making. (2) By mapping the flood inundation area, we can effectively identify the spatial differentiation characteristics of the flood hazard so as the characteristics of sensitive groups and environment, and provide a reference for the spatial layout of emergency disaster reduction and prevention facilities to strengthen urban adaptability.

Keywords

Flood inundation area mapping, Threshold-based extraction, Extreme rainfall event

1. Introduction

Climate change, one of the most severe challenges facing mankind today, is a major global issue of general concern to the international community, which is also the direct result of the massive creation of material wealth on an unprecedented scale. The impact of climate change is mainly referred to extreme weather and climate events, such as floods, droughts, and sea-level rise, affecting natural and human systems including life, livelihood, health, ecosystem, economy, society, culture, services, and infrastructure. The impact of recent climate-related extreme events (such as heatwaves, droughts, floods, cyclones, and wildfires) has revealed the serious vulnerability and exposure of ecosystems and human systems to current climate change(Field *et al.*, 2014). The concept of “climate adaptation” originated from concerns about the long-term effects of climate change. As early as the 1990s, the Intergovernmental Panel on Climate Change (IPCC) began to study the impact of climate change and extreme weather in different scenarios. In 2007, the IPCC officially explained the concept of “climate adaptability” in its work report, emphasizing that in the context of the gradual acceleration of climate change and the increasingly significant impact of climate, “natural or human systems’ or its impact, need to respond to mitigate the harm caused by climate change or seek favorable opportunities"(Ipcc, 2007).

Floods are one of the most dangerous and frequent natural hazards. From 1970 to 2012, floods accounted for 79% of the total natural disasters reviewed, resulting in 55% of deaths and 86% of economic losses (Organization, 2014). The frequency of flood disasters on a global scale has an increasing trend from 1970 to 2018 (Hu *et al.*, 2018), causing more and more life and property loss. In 2005, the Hurricane Katrina storm surge disaster chain in the United States broke the flood control dike in New Orleans, and the economic loss reached more than 96 billion $ (Lagadec, 2006). In 2008, Tropical Storm Nargis swept across the delta of Myanmar, killing 138,000 people (Shibayama, 2015). In addition, Typhoon Haiyan in the Philippines (2013), Hurricane Sandy in New York (2012), and Hurricane Harvey in Texas (2017) have caused huge casualties and economic losses.

Recently, Xinxiang City in Henan Province has experienced extremely heavy rainstorms since July 17, 2021. Xinhua News Agency reported on the 22nd that from 8:00 on July 17 to 6:00 on the 22nd, there was a heavy rainstorm in Xinxiang, with a maximum precipitation of 907 mm. Among the 175 sites in the city, 14 sites are above 700 mm, 26 sites are 600-700 mm, 26 sites are 500-600 mm, and 37 sites are 400-500 mm. The maximum one-hour rain intensity is 149.9 mm, and the maximum two-hour rain intensity is 267.4 mm. The period of the strongest precipitation occurs from 5 o'clock on the 20th to 5 o'clock on the 22nd, with precipitation of 812 mm. The economic losses amounted to approximately $65.25 million. But the extent of flood impact in Xinxiang City uring the extreme weather event remains to be discussed.

Effective flood disaster monitoring and management are critical to minimize loss of life, property, and infrastructural damage, industrial, agricultural, and other losses(Doki *et al.*, 2020). What's more, The timely information of the flood area and impacts are helpful for the government to act immediately to emergency response. The rapid estimation of the spatial extent of flooding over large areas provides a key data source for assessing the disaster risk and climate adaptation planning(Dumitru *et al.* 2014). Mapping the flooding areas is also effective to identify the spatial differentiation characteristics of the flood risk, so as the characteristics of sensitive groups and environment, and provide a reference for the spatial layout of emergency disaster reduction and prevention facilities to strengthen urban adaptability. In this respect, adopting advanced methods to extract flood inundation areas is one of the most primary and essential tasks for climate adaption planning.

Satellite-based observation maps can provide the temporal and spatial distribution and range of floods with various spatial resolutions, and nearly in real-time(Zhang *et al.*, 2021). There are two types of satellite observations that can be used to monitor flood inundation areas: optical images and synthetic aperture radar (SAR) images. Optical remote sensing images such as NOAA(Wang *et al.*, 2003), MODIS(Peng, 2004), Landsat MSS(Renó *et al.*, 2011), Landsat TM(Giuliana *et al.*, 1997), and HJ are available to monitor and extract the flood inundation areas. However, However, due to the long duration of cloudy and rainy weather, the optical remote sensing satellite will be blocked for a long time during monitoring, and the actual situation of large-area underlying surface cannot be observed accurately and effectively(Cian *et al.*, 2018). Therefore, optical remote sensing has some limitations in the accuracy and timeliness of flood monitoring(Cui *et al.*, 2020) (). The SAR image with the high spatial resolution has the ability of all-weather observation and is not affected by clouds and rain, which acquired better contrast and rich texture information, greatly improves the monitoring efficiency and accuracy(Huth *et al.*, 2020). Unlike the optical data, SAR data can detect the geochemical properties of the ground surface such as surface roughness and dielectric constant(Singha *et al.*, 2020). Hence, SAR data are better for classifying different flood situations such as flooded open areas, flooded urban areas, and flooded vegetation(Gašparović *et al.*, 2020; Li *et al.*, 2019).

Several SAR-based flood detection techniques have been successful applied to flood mapping(Matgen *et al.*, 2011; Martinis *et al.*,, 2015; Cossu *et al.*, 2009). There are three mainstream methods of extracting urban flood areas. One is based on the SAR interferometric coherence(γ) (Rimba and Miura, 2017; Tanguy *et al.*, 2017; Patias *et al.*, 2021; Twele *et al.*, 2016). Interferometric coherence, which indicates the

correlation of two complexes (amplitude and phase) observations, provides additional information for urban flood mapping since an urban settlement can generally be considered a stable target characterized by high coherence (Zhang *et al.*, 2021; Brisco *et al.*, 2015). Another is classified based on object or pixel, including KNN classifier, Maximum likelihood classifier, Minimum distance to mean distance classifier, KD Tree KNN classifier, Random Forest classifier(Geetha *et al.*, 2018). The third one is based on the threshold. A dynamic threshold method (Otsu's method) is used to distinguish water bodies and non-water bodies (Qiu *et al.*, 2021).

For China, some scholars have carried out relevant research. A combination of optical image (Landsat 8) and SAR (COSMO-SkyMed) images was used to map floods using support vector machine classifiers in China(Tong *et al.*, 2018). Otsu's method is employed to investigate floods and explore flood patterns across the Pearl River Basin, Chian from 2017 to 2020. Xianlong Zhang et al., 2021 investigate the use of an object-oriented classification approach for flood information monitoring in floodplains in Poyang Lake, Jiangxi Province, China. Hyun-Ju Ban et al., 2017 adopted RGB composite techniques using advanced sensors with more bands and higher spatiotemporal resolutions for estimating flood events in Wuhan, China(Ban *et al.*, 2017). However, seldom researches focus on the Spatial extent and impact of floods under extreme weather events in non-flooded plains. In our study, to increase the flood identification timeliness, we used a threshold-based method to quickly extract the flood area. This method has been proven to be effective.

Our objective was to map flood inundation areas using Sentinel-1 SAR images through SNAP and ENVI platforms and analyze their spatial characteristics. We would like to answer the following research questions: (1) what is the extent of flood impact? (2) what are the spatial characteristics of the flood inundation areas? The remainder of this paper is structured as follows. Section 2 introduces the study area, workflow, datasets, and data processing. Section 3 introduces the results of the flood inundation map and flood variation characteristics and provides discussions. Finally, Section 4 concludes this paper.

2. Method

2.1 Study Area

Our study area includes parts of Xinxiang City, Anyang City, and Hebi City in Henan Province, China, and the major part of our study area is located in Xinxiang City.

Xinxiang City is located in the hinterland of the Central Plains and the north of Henan Province. Its geographical coordinates are 113°23′-115°01′E and 34°53′-35°50′N. Its center is 35°18′N and 113°54′E. It faces the Yellow River in the South and faces Zhengzhou and Kaifeng across the river. It is adjacent to Taihang City, Hebi City, and Anyang City; It connects Jiaozuo City, the hometown of Tai Chi in the west, and borders Southeast Shanxi. It is connected to the oil city Puyang in the East and Luxi in the West. The total area is 8249 km^2. Xinxiang City has a warm temperate continental monsoon climate with four distinct seasons, cold in winter and hot in summer, cool in autumn and early in spring, and the average temperature over the years is 14℃. July is the hottest, with an average of 27.3°C. January is the coldest, with an average of 0.2°C.

The average annual precipitation in Xinxiang City is 573.4mm, and the variation range among counties is 549.9 - 644.4mm. The less rainy center is Yuanyang, and the more rainy center is located in the Huixian mountain area in the northwest. The seasonal distribution of precipitation is very uneven, which is roughly consistent with the advance and retreat of winter and summer monsoon. The first day of frost in the city mostly occurs in late October, and the whole day mostly occurs in early April. The average annual frost-free period is 205 days.

Xinxiang City belongs to the two major water systems of the Haihe River and Yellow River. It is an area with few water sources. It is located on the North Bank of the lower reaches of the Yellow River, mostly on the

north wing of the alluvial fan plain of the Yellow River. The Yellow River enters from Yaokou village, Yuanyang County, and exits from Changyuan City. The river is 165 km long and the dike is 153 km long. The rivers on the surface alluvial fan sector in the territory take the ancient Yellow River (Yu River), the aboveground suspended river flowing from southwest to northeast in the Western Han Dynasty, as the watershed. The ancient river channel is 2 - 4m higher than the ground. It is in the line of Yuanyang Zhulou, Heiyangshan - Baliushu, Xinxiang County, Huguzhai - Dongtun, Yanjin - Weihui Pangzhai - Fengzhuang, Yanjin. Haihe River system is located in the northwest of Xinxiang, with a drainage area of 3985 kilometers, and the Yellow River system is located in the southeast, with a drainage area of 4184 km^2. The study area is about 3543.53 km^2.

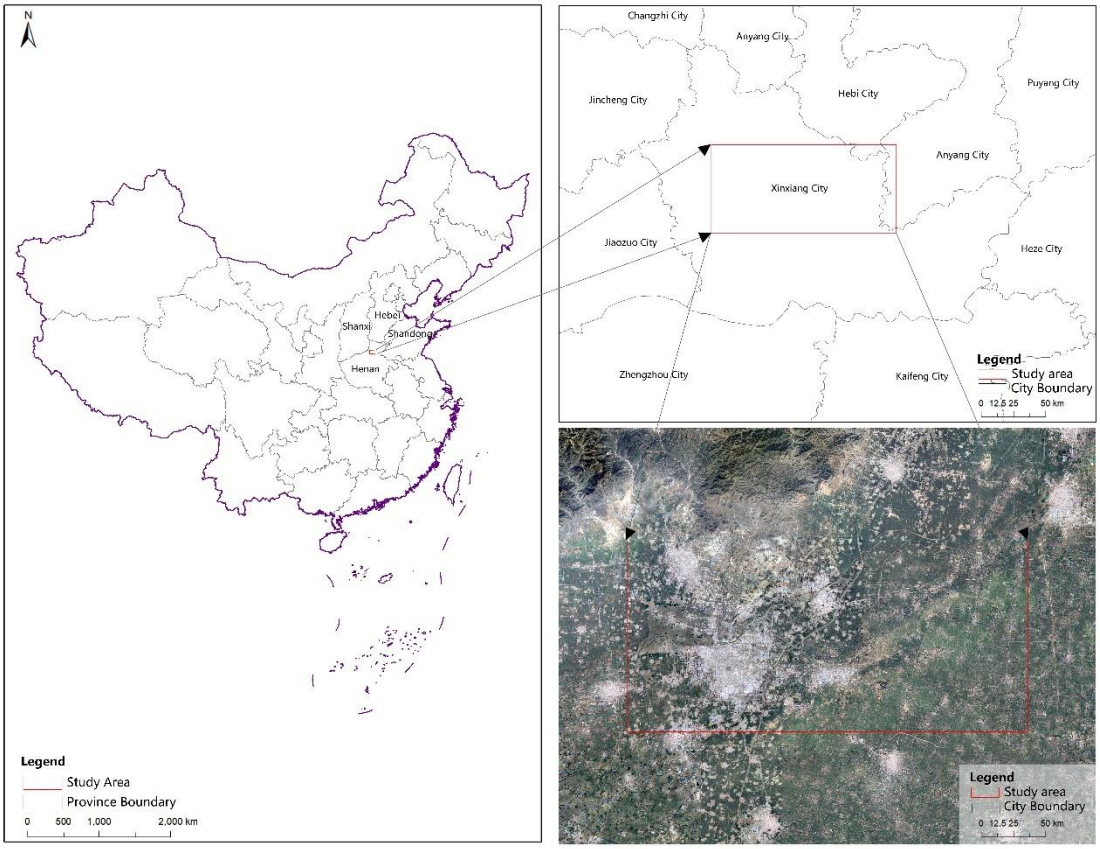

Figure 1 Study area

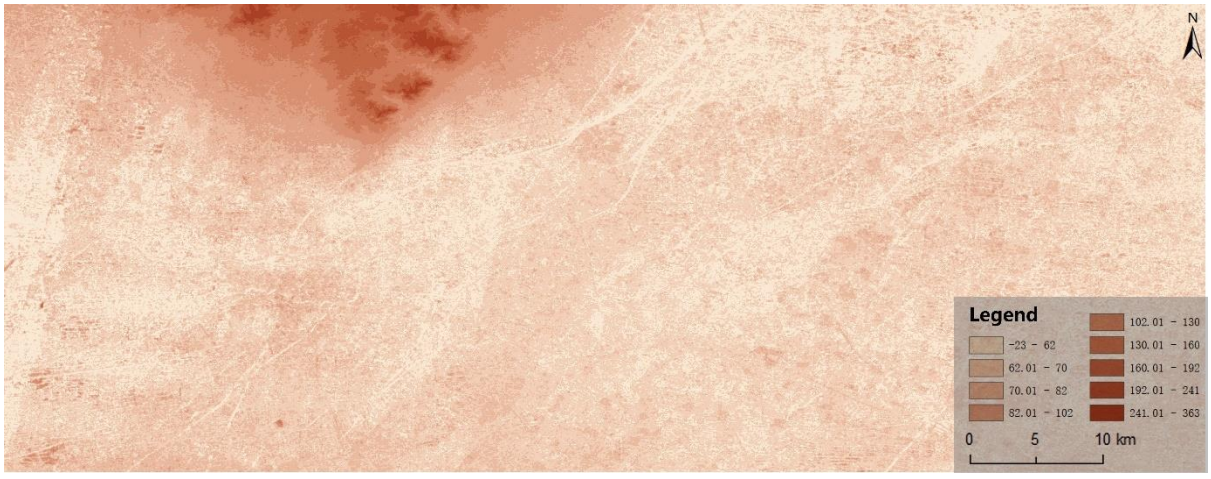

Figure 2 DEM of the study area

2.2 Workflow

The methodology of this study includes the following key components (Figure 3): (1) origin image pre-processing on the SNAP; (2) find the permanent water bodies on the pre-flood image, and find the extended waterbodies on the post-flood image, the identification of water bodies using the Sentinel-1 SAR data by threshold-based extraction, then identify the flood inundation area by extraction the difference of permanent water bodies and extended waterbodies; (3) validation the accuracy of the pre-flood waterbodies and post-flood waterbodies by Google Map; (4) analyze the characteristics of the flood inundation area.

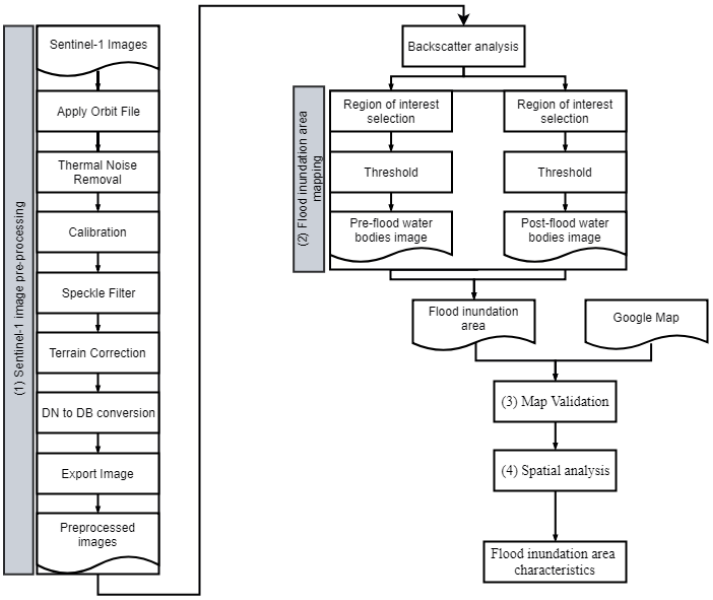

Figure 3 Methodology

2.3 Datasets

In this study Sentinel level-1 Ground Range Detected (GRD) data were acquired in Copernicus open access hub (European Space Agency). The mission of Sentinel level-1 comprised of two polarizations of VV/VH performing C-band Synthetic Aperture Radar (SAR) frequency of 5.404 GHz available in all kinds of weather situations of day and night time with a revised period of 12 days.

This study used 8 Sentinel-1 interferometric wide (IW)-mode images in VV polarization channel collected from 8 July 2021 to 8 August 2021, in conjunction with the NASA Shuttle Radar Topography Mission (SRTM) Digital Elevation Model(DEM). Table. 1 lists specific information about the Sentinel-1 data used in this study (Table. 1).

Table. 1 Data Acquisition

Acquisition	Flight direction	Absolute orbit	Note
2021/07/15	Ascending	38787	Pre-flood
2021/07/27	Ascending	38962	Post-flood

2.4. Data processing

2.4.1 SAR data pre-processing

The Sentinel level-1 Ground Range Detected (GRD) raw data were pre-processed in Sentinel Application Platform(SNAP), which is freely provided by the European Space Agency(ESA) for the scientific exploitation

of Earth Observation missions under the Scientific Exploitation of Operational Missions(SEOM). The data were pre-processed as follows: Subsetting the raw data based on the research scope to improve the calculation efficiency and reduce the backscattering interference of other ground objects, applying orbit file to precise the data for better geocoding progress, the radiometric calibration toolbox is used to convert the pixel into radar backscatter coefficient. Speckle filtering is a procedure to increase image quality by reducing speckles. The speckle filtering method uses the spatial correlation of the image pixels to filter the coherent speckle noise. Generally, a sliding window is used, and the pixels in the window are weighted to obtain the pixel value at the center of the window(Gondwe *et al.*, 2020). Refined Lee filter is the most commonly used coherent speckle filter, which can be automatically adjusted according to the study area. The undulations of ht terrain will cause significant geometric distortions in the SAR image, leading to shrinkage, overlap, shadows, and other phenomena. Converting DN to DB is the last step of the preprocessing workflow. The unitless backscatter coefficient is converted DB by using a logarithmic transformation as follows:

$$\sigma_{dB} = 10 \times \lg(DN)$$

Where DN value is the gray value of image pixels and dB is the backscattering coefficient.

The preprocessed image was exported for classification (Figure 4 and Figure 5). All processing steps were assembled and connected through Graph Builder, which is provided in SNAP and runs in batch mode.

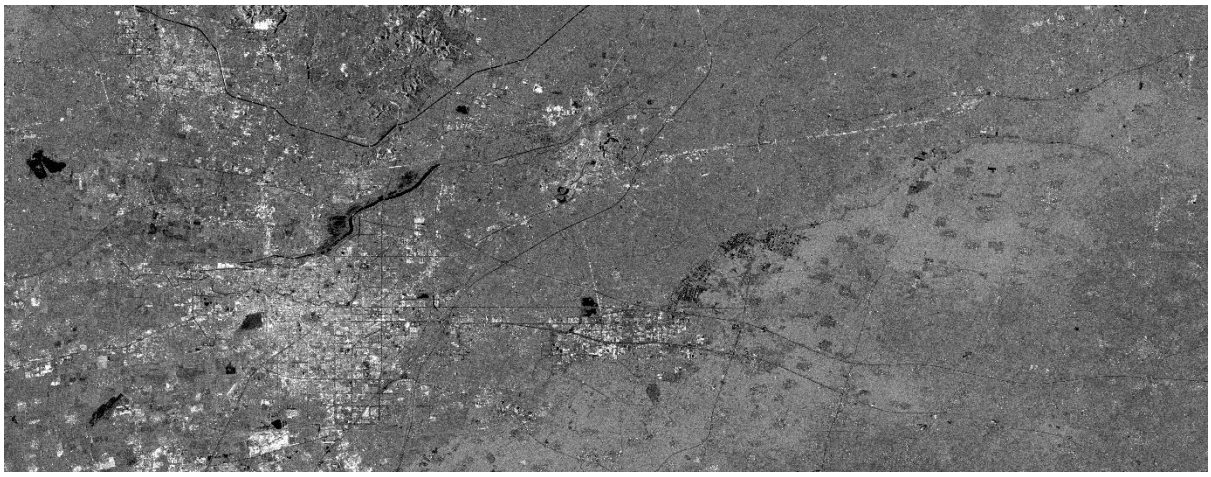

Figure 4 preprocessed result of pre-flood image

Figure 5 preprocessed result of post-flood image

2.4.2. Mapping the flood inundation area

The preprocessed images were imported into the ENVI platform for threshold-based extraction. In this study, we adopted the single threshold method, which has the advantages of simple principle, convenient operation, easy understanding, saving time, and meeting the timeliness requirements of writing service materials. It is well known that an open water surface will lead to a low backscattering coefficient because of the specular reflection of the SAR signal on the water surface and the high permittivity of water(Sensing, 1981). The radar backscatter over urban surfaces is higher than water surfaces. In the pre-flood image and post-flood image, the surface backscattering coefficient corresponding to the same pixel will be different in different phases, so the threshold of water extraction for these two phases is different. We drew the ROI of water on the pre-flood image and post-flood image to analyze the threshold of water backscattering at different times. We use the histogram to analyze the water backscattering coefficient in these two phases image(Figure 6). The pre-flood threshold value is -23.262918 dB to -12.796155 dB. The post-flood threshold value is -25.319732 dB to -14.522955 dB. The above steps were all performed on the ENVI platform.

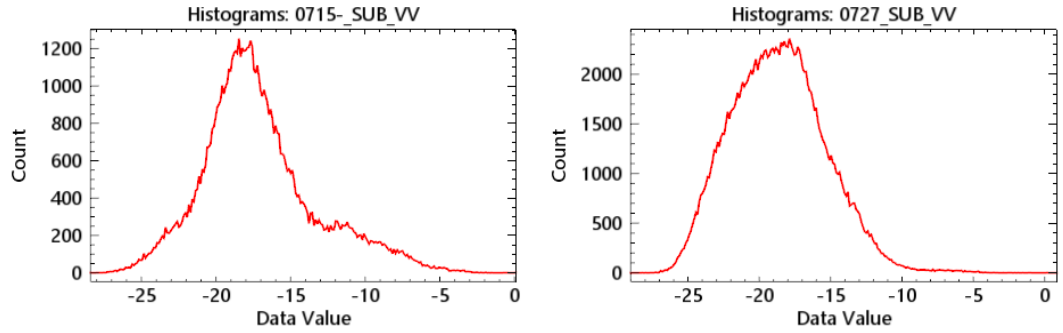

Figure 6 Histograms of VV in the pre-flood image (a) and Histograms of VV in the post-flood image(b)

2.4.3. Accuracy assessment of flood inundation map

To verify the accuracy of sentry 1 monitoring results, the Google Map is used to monitor the flood inundation area. We generate 1000 random checkpoints on the ArcGIS platform to assess the accuracy (Figure 7), and the overall accuracy is 85.47%.

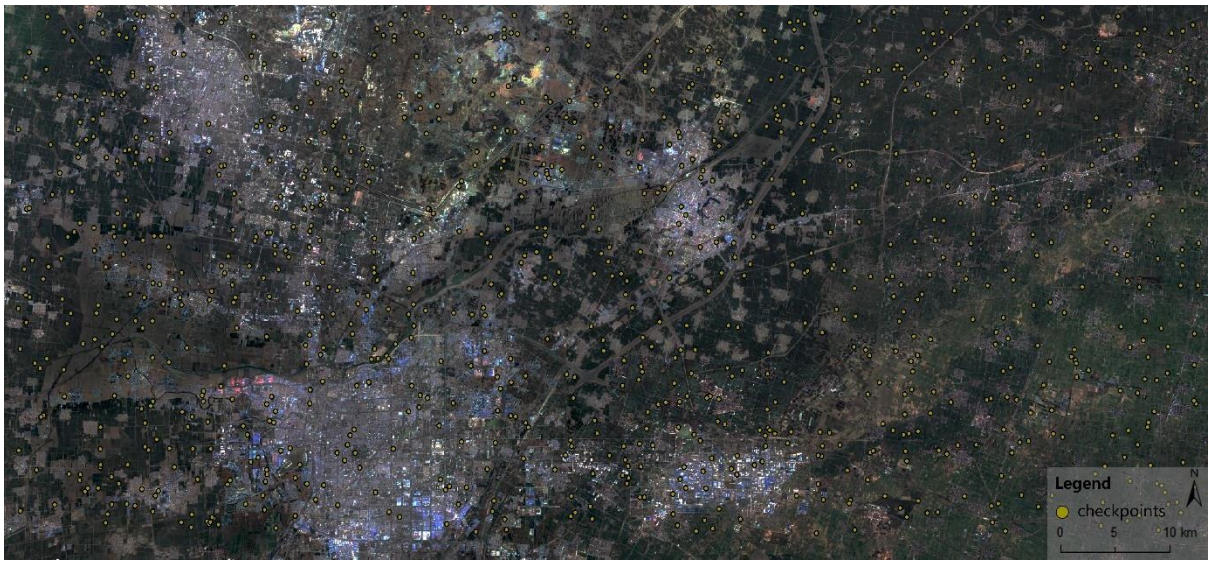

Figure 7 checkpoints

3. Results and Discussion

3.1 Results

After preprocessing the collected data set, backscatter analysis will display the backscatter reflectance of the water body. Through the possibility of automatic processing chain based on SAR, flood inundation area mapping based on the sentinel-1 image has the potential to quickly provide flood information for flood management. During flood mapping, significant differences in backscatter values between water and non-water areas can separate the flood area from other land areas. The backscatter response of pre-flood image in VV polarizations for water bodies showed a range between -23.262918 dB and -12.796155 dB. The backscatter response of post-flood image in VV polarizations for water bodies showed a range between -25.319732 dB and -14.522955 dB.

Figure 8 and Figure 9 showed the extent of the water body extracted by the proposed method. The results showed the presence of perennial water bodies on July 15 2021 covering an area of 1.58%. On July 27, 2021, the total waterbodies area was 5.41%. Table. 2 showed that in the post-flood image, the area of the water bodies increased 242.85% than the pre-flood image, which indicated that the extreme weather events have had a greater impact.

Overlaid the water bodies of pre-flood and post-flood images, in which light blue indicated the perennial water bodies and red indicated the flood inundation area (Figure 10), which can monitor the changes of the water body. The flood inundation area was about 135.73 km^2, occupying 3.83% of the study area. The flood inundation area is mainly located on the northeast part of the study area, and also along with the Weihe River, with most flood inundation areas occurring in farmland, urban and rural settlements.

We selected some main flood inundation areas in Figure 11 and analyzed the elevation, land cover on the Google Map to analyze the characteristics of the flood inundation area, and other properties of them. It was obvious that the elevation (Table. 3) of the four main flood inundation areas is lower than the average elevation of the study area (71.88m). What's more, comparing the standard deviation of the elevation of the four main flood inundation areas to the total of the study area (23.69), the elevation fluctuations of the four main flood inundation areas are small. Therefore, it's supposed that elevation is a key factor affecting the flood inundation area. Figure 12 showed the landcover of the flood inundation area, which are mainly dryland, followed by paddy field. The flood caused great agricultural damage.

Table. 2 Waterbodies area and proportion before and after the flood

	Waterbodies area(km^2)	Percentage
Pre-flood image	55.89	1.58%
Post-flood image	191.62	5.41%
Flood inundation image	135.73	3.83%

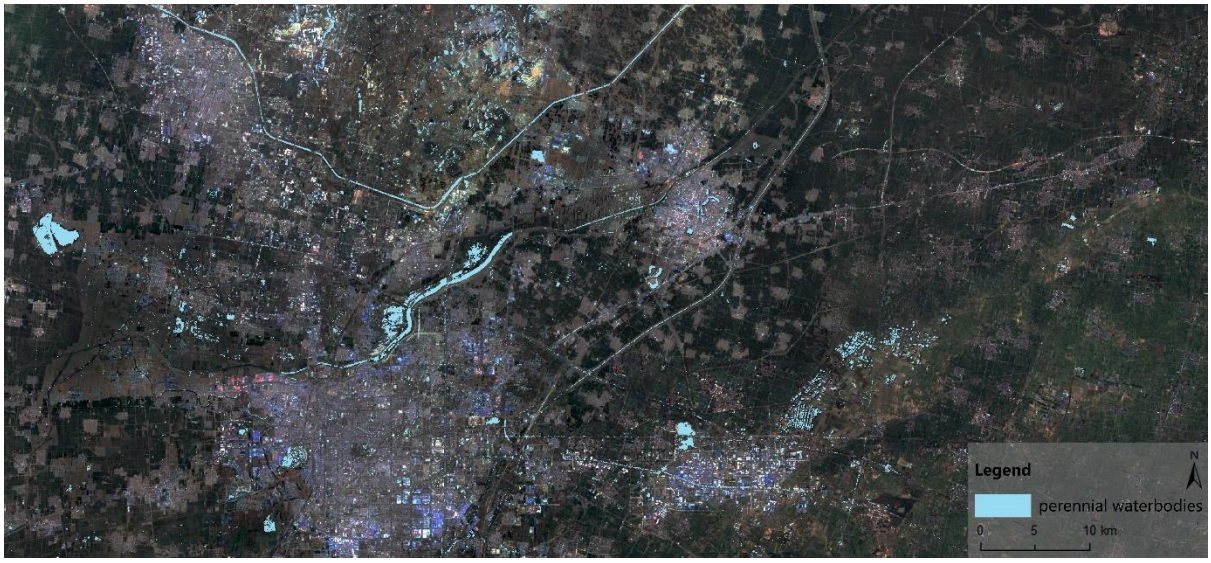

Figure 8 perennial waterbodies

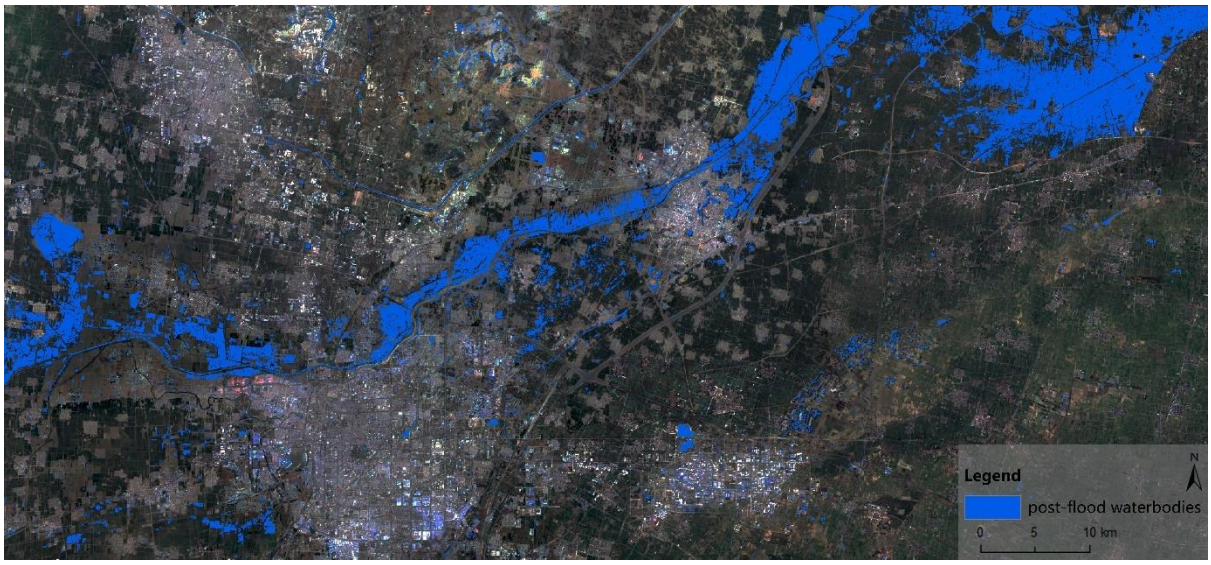

Figure 9 post-flood waterbodies

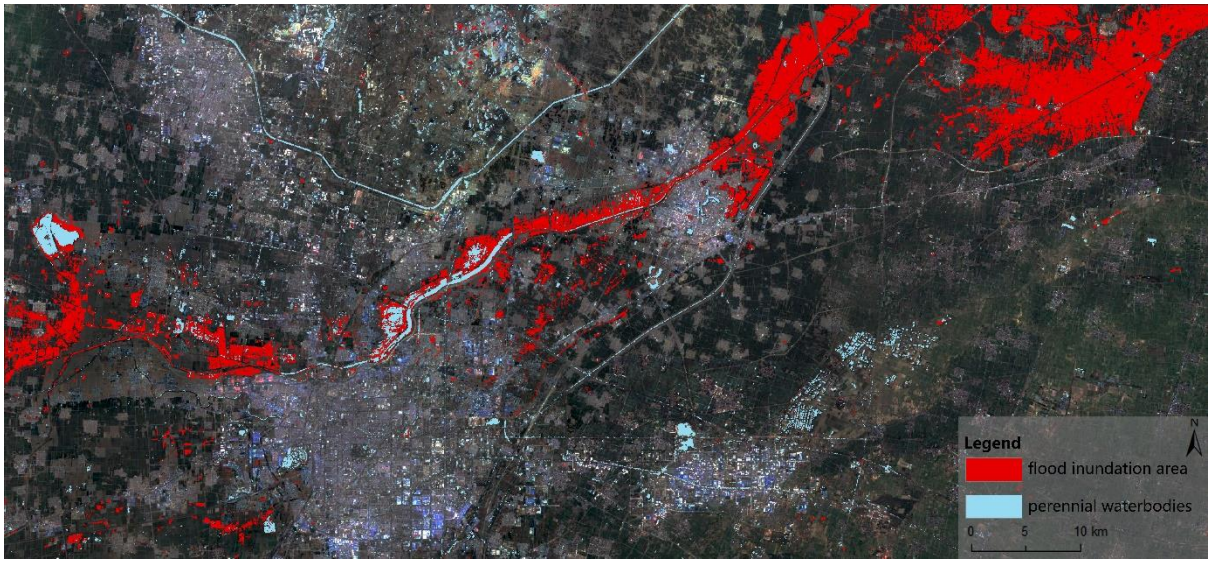

Figure 10 The flood inundation map

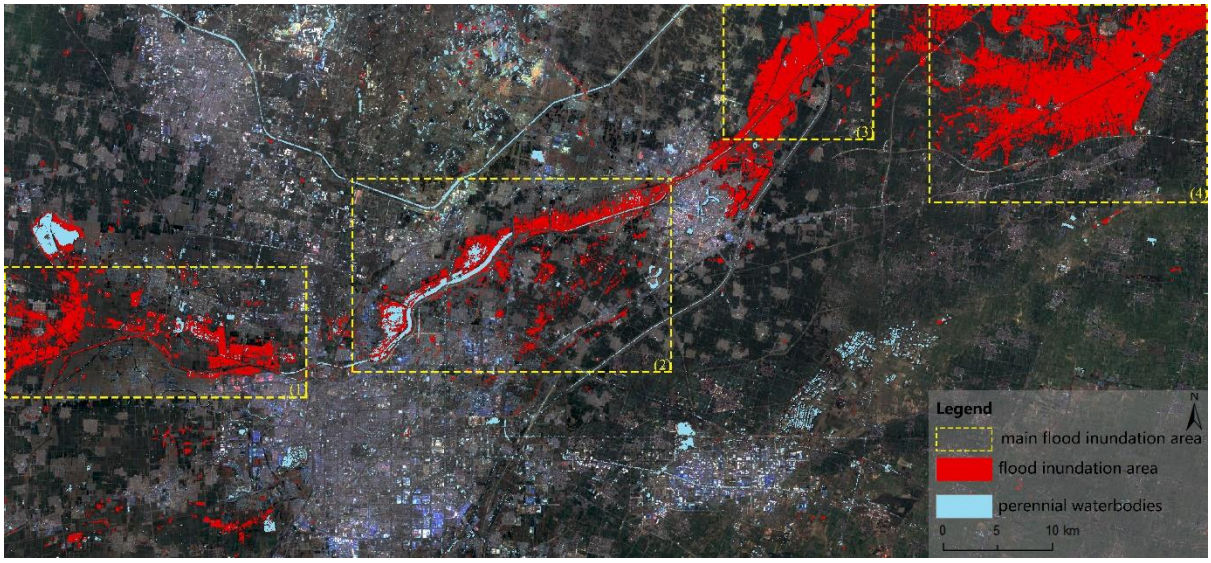

Figure 11 The main flood inundation area map

Table. 3 Elevation of the main flood inundation area

ID	Landcover	Average elevation(m)	The standard deviation of elevation
(1)	farmland	60.29	8.77
(2)	farmland	62.64	5.35
(3)	farmland	61.65	5.51
(4)	farmland	62.31	7.49

Main flood inundation area (1)

Main flood inundation area (2)

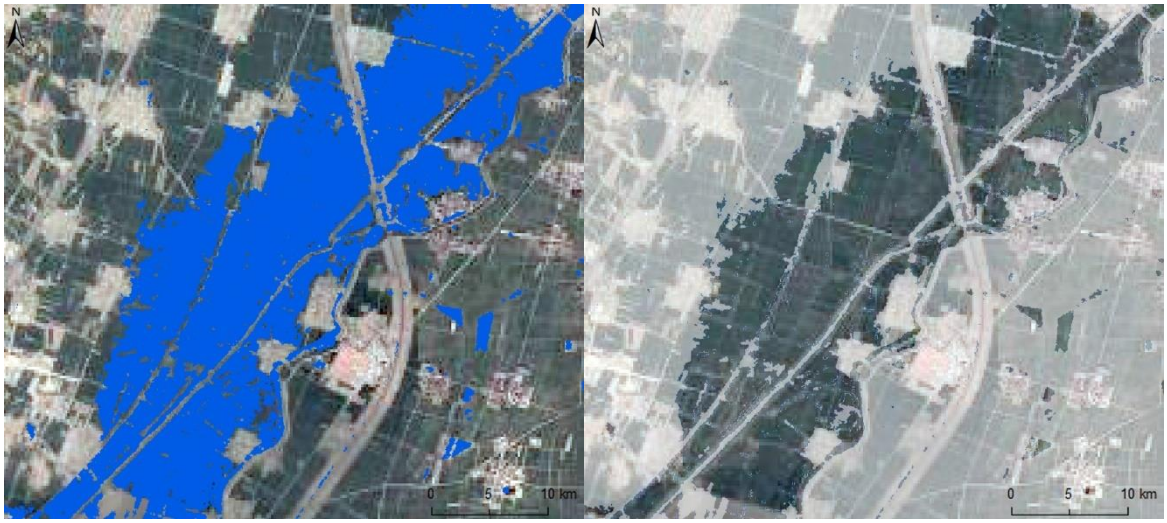

Main flood inundation area (3)

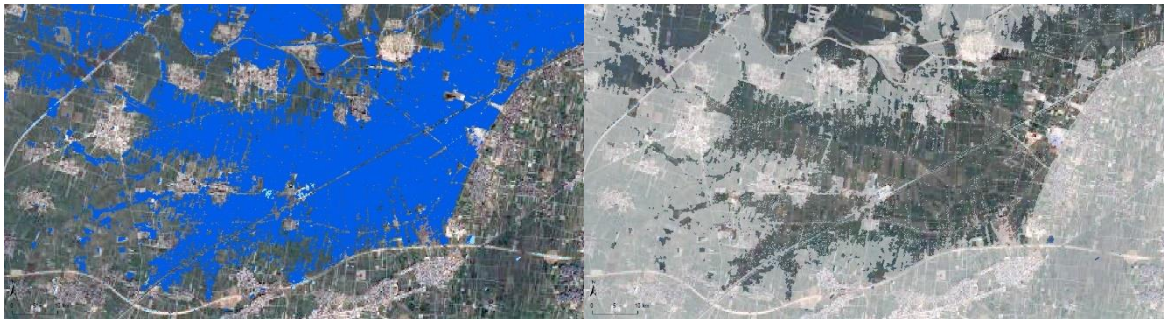

Main flood inundation area (4)

Figure 12 The google map of the main flood inundation area

3.2 Discussion

Sentinel-1 SAR satellite is a C-band sensor specification launched for natural events in the environment and various applications. SAR data is provided free of charge, mainly with 10m high resolution. SAR data is cloud penetrating data available under various weather conditions and day and night time. It is an effective tool for mapping natural disasters, with a time resolution of 12 days. In the time of disaster acquisition of image depending on the satellite pass availability.

The heavy rainfall event in July triggered the flood disaster in Xinxiang City, Henan Province to a large extent, with most flood inundation areas occurring in farmland, urban and rural settlements. The disadvantage of the agricultural pattern in the study area is that the farming methods and land use methods are unscientific, such as wetland to dry land, and the river area is built into a built-up area. The improper drainage system is also an important cause of flood in case of an accident, so major losses mainly occur in farmland and residential areas.

Mapping the flood inundation area of non-flooded plains under extreme weather is of great significance because climate change has caused higher flood frequences in non-flooded plains, which should draw public attention. More and more floods will destroy lives, livestock, and infrastructure and bring huge economic losses as the climate change. During a flood disaster, access to reliable information is crucial. In addition to wall-to-wall comparison with optical or field studies, the use of SAR images to estimate the degree of flood in non-flood plain areas can also be used for disaster management purposes such as disaster relief. The urban systems in non-flooded plains have poor adaptability to extreme weather. In the past, these non-flooded plains relied on dams to deal with flood risks, which is not sustainable. Based on

data-driven, it provides an operable technical process and method for rainwater hazard mapping of climate adaptability planning for non-flood plains in China, which can be applied to rainwater hazard mapping of other areas and enhance the science of decision-making. By mapping the flood inundation area, we can effectively identify the spatial differentiation characteristics of the flood risk, so as the characteristics of sensitive groups and environment, and provide a reference for the spatial layout of emergency disaster reduction and prevention facilities to strengthen climate change adaptability.

As part of the operation method, the flood inundation area will be better to be verified using Landsat 8 images. But, unfortunately, due to the dominance of cloudy conditions, free-cloud Landsat images are not available at the peak of the flood.

4. Conclusion

This study demonstrates the use of a simple technique to estimate the VV polarization of SAR data of flood inundation range. The band mathematical-statistical method will use an ROI mask to estimate the threshold in the flood inundation area of the SAR dataset. According to the principle of radar imaging, the threshold-based extraction method is used to quickly extract the flood inundation area seriously affected by the heavy rainstorm in Xinxiang City from July 15 to 27, 2021. This demonstration technique is a visual interpretation of the results that are generally applicable and emphasize the effect of methodology.

Through the research, the following conclusions are drawn: 1) the threshold-based extraction method can quickly distinguish the water bodies and non-waterbodies, the difference between water and land boundaries is obvious, and the water body information before and after the disaster is obvious, The experimental results meet the accuracy-test; 2) Sentry 1 data has good detection ability for surface water information, short return visit cycle, simple and effective research method, and can professionalize the rainstorm disaster assessment and judgment; 3) the low elevation and farmland along the river are the key characteristics of the flood inundation area, and the vulnerability assessment of crops and agriculture should be strengthened; 4) In this paper, to improve the accuracy of calculation area, it is necessary to further eliminate the influence of reference water areas such as small tributary water body and target shadows such as mountains and buildings.

This research focuses on non-flooding plains caused by extreme precipitation events under the background of climate change. By drawing lessons from previous methods, a method of flood inundation area identification is proposed based on SAR images that is quick and operable for urban planners. It is a basic link in climate adaptability planning and helps to identify flood space characteristics, which improves the adaptability of non-flooded plain cities to flood disasters under the background of climate change.

There are also some limitations to our study. First, lack of field survey data for map validation. Second, the factors of the flood inundation area we have considered are not enough, we will combining multi-source data such as POI, people density in the future study. Third, this study lacks hydrological analysis and cannot analyze the flood expansion path.

References

Ban, H. J. *et al.* (2017) 'Flood monitoring using satellite-based RGB composite imagery and refractive index retrieval in visible and near-infrared bands', *Remote Sensing*, 9(4). doi: 10.3390/rs9040313.

Brisco, B. *et al.* (2015) 'Evaluation of RADARSAT-2 Acquisition Modes for Wetland Monitoring Applications', *Canadian Journal of Remote Sensing*, 41(5), pp. 431–439.

Cian *et al.* (2018) 'Normalized Difference Flood Index for rapid flood mapping: Taking advantage of EO big data', *Remote Sensing of Environment: An Interdisciplinary Journal*, 209, pp. 712–730.

CO Dumitru, S Cui, M Datcu (2014) 'Quantitative flood assessment: Case study of floods in Germany', in *IGARSS 2014*.

Cossu, R. *et al.* (2009) 'Near real-time SAR-based processing to support flood monitoring', *Journal of Real-Time Image Processing*, 4(3), pp. 205–218.

Cui, J. *et al.* (2020) 'Integration of optical and SAR remote sensing images for crop-type mapping based on a novel object-oriented feature selection method', *International Journal of Agricultural and Biological Engineering*, 13(1), pp. 178–190.

Doki, D. *et al.* (2020) 'The Impact of Trade Balance of Agri-Food Products on the State's Ability to Withstand the Crisis'.

Field, C. B., Barros, V. R. and Change, I. P. C. (2014) 'IPCC, 2014: Climate Change 2014: Impacts, Adaptation, and Vulnerability. Part A: Global and Sectoral Aspects. Contribution of Working Group II to the Fifth Assessment Report of the Intergovernmental Panel on Climate Change', *guangdong agricultural sciences*.

Gašparović, M. and Dobrinić, D. (2020) 'Comparative Assessment of Machine Learning Methods for Urban Vegetation Mapping Using Multitemporal Sentinel-1 Imagery', *Remote Sensing*, 12(12), p. 1952.

Geetha Priya, M. and PriyaM, D. (2018) *Supervised classification for flood extent identification using sentinel-1 radar data FLOW BATTERY DESIGN View project REVERSIBLE COMPUTING View project Supervised classification for flood extent identification using sentinel-1 radar data*. Available at: https://www.researchgate.net/publication/330441584.

Giuliana, P. and Heather, M. (1997) 'Flood management through LANDSAT TM and ERS SAR data: a case study', *Hydrological ProcHydrological Processesesses*.

Gondwe, S. and Shukla, S. (2020) 'Mapping Flood Risk of Nsanje District in Malawi Using Sentinel-1 Data SEE PROFILE'. doi: 10.37591/.v11i3.1066.

Hu, P. *et al.* (2018) 'Flood-induced mortality across the globe: Spatiotemporal pattern and influencing factors', *Science of The Total Environment*.

Huth, J. *et al.* (2020) 'Analyzing water dynamics based on sentinel-1 time series-a study for dongting lakewetlands in China', *Remote Sensing*, 12(11). doi: 10.3390/rs12111761.

Ipcc, C. (2007) 'Climate Change 2007: Mitigation. Contribution of Working Group III to the Fourth Assessment Report of the Intergovernmental Panel on Climate Change', *Computational Geometry*, 18(2), pp. 95–123.

Lagadec, P. (2006) 'The Federal Response to Hurricane Katrina – Lessons Learned'.

Li, Y., Martinis, S. and Wieland, M. (2019) 'Urban flood mapping with an active self-learning convolutional neural network based on TerraSAR-X intensity and interferometric coherence', *ISPRS Journal of Photogrammetry and Remote Sensing*, 152(JUN.), pp. 178–191.

Martinis, S., Kersten, J. and Twele, A. (2015) 'A fully automated TerraSAR-X based flood service', *ISPRS Journal of Photogrammetry and Remote Sensing*, 104, pp. 203–212.

Matgen, P. *et al.* (2011) 'Towards an automated SAR-based flood monitoring system: Lessons learned from two case studies', *Physics & Chemistry of the Earth*, 36(7–8), pp. 241–252.

Organization, W. M. (2014) 'Atlas of mortality and economic losses from weather, climate and water extremes (1970-2012).', *World Meteorological Organization*.

Patias, N. *et al.* (2021) 'Sustainable urban development indicators in Great Britain from 2001 to 2016', *Landscape and Urban Planning*, 214. doi: 10.1016/j.landurbplan.2021.104148.

Peng, D. Z. (2004) 'Analysis of the influence of Dongting Lake's area variation measured by MODIS on flood level', *Yangtze River*.

Qiu, J. *et al.* (2021) 'Flood monitoring in rural areas of the pearl river basin (China) using sentinel-1 SAR', *Remote Sensing*, 13(7), pp. 1–21. doi: 10.3390/rs13071384.

Renó, V. F. *et al.* (2011) 'Assessment of deforestation in the Lower Amazon floodplain using historical Landsat MSS/TM imagery', *Remote Sensing of Environment*, 115(12), pp. 3446–3456.

Rimba, A. B. and Miura, F. (2017) 'Evaluating the Extraction Approaches of Flood Extended Area by Using ALOS-2/PALSAR-2 Images as a Rapid Response to Flood Disaster', *Journal of Geoscience and Environment Protection*, 05(1), pp. 40–61.

Sensing, M. R. (1981) 'Microwave remote sensing', *Addison-Wesley Pub. Co*.

Shibayama, T. (2015) 'Field Surveys of Recent Storm Surge Disasters', *Procedia Engineering*.

Singha, M. *et al.* (2020) 'Identifying floods and flood-affected paddy rice fields in Bangladesh based on Sentinel-1 imagery and Google Earth Engine', *ISPRS Journal of Photogrammetry and Remote Sensing*, 166(January), pp. 278–293. doi: 10.1016/j.isprsjprs.2020.06.011.

Tanguy, M. *et al.* (2017) 'River flood mapping in urban areas combining Radarsat-2 data and flood return period data', *Remote Sensing of Environment*, 198, pp. 442–459.

Tong, X. *et al.* (2018) 'An approach for flood monitoring by the combined use of Landsat 8 optical imagery and COSMO-SkyMed radar imagery', *Isprs Journal of Photogrammetry & Remote Sensing*, 136(FEB.), pp. 144–153.

Wang, Q. *et al.* (2003) 'Using NOAA AVHRR data to assess flood damage in China.', *Environmental Monitoring & Assessment*, 82(2), pp. 119–148.

Zhang, X. *et al.* (2021) 'Mapping flood by the object-based method using backscattering coefficient and interference coherence of Sentinel-1 time series', *Science of the Total Environment*, 794. doi: 10.1016/j.scitotenv.2021.148388.